Synthesis and Characterization of Au/Fe_3O_4 NCs Decorated Graphene Oxide via Pulsed Laser Ablation Technique

Basma Said, Horia. F., M. Nabil, Said Abdallah, and Sohair Negm

[a] *Basic Engineering Sciences department, Faculty of Engineering, Benha University, Egypt*

The demand for nanocomposites (NCs) of graphene and magnetite materials decorated with gold nanoparticles is increasing on account of their applications in science and technology. First, graphene oxide (GO) was made with the pulsed laser ablation technique in liquid (PLAL) and then loaded with magnetite (Fe_3O_4) that was prepared by the same technique to form Fe_3O_4/GO nanocomposite (NCs). The Au/Fe_3O_4 NCs were also synthesized and added by volume ratio to the GO solution to form Au/Fe_3O_4/GO NCs. We investigated the functional groups in the three samples using Fourier transform infrared spectroscopy (FTIR). We measured the optical absorption spectra of the samples using UV-visible light. From these optical spectra, we calculated the optical conductivity (σ), absorption coefficient (α), and other related optical properties. We improved the optical absorption and other optical parameters while decreasing the band gap (Eg) from 4.1 eV to 3 eV for the three samples. These materials are suitable for photonic applications, drug delivery applications, and water treatment applications.

Keywords

graphene oxide (GO), magnetite (Fe_3O_4), gold/magnetite NCs, and the pulsed laser ablation technique.

Corresponding Author: drnegm@hotmail.com

Receive Date: 8 March 2025; Revise Date: 12 April 2025; Accept and Publish Date: 29 April 2025

Introduction

A layered carbon structure with functional groups including oxygen is called graphene oxide (GO). Graphene oxide (GO) contains various types of oxygen groups, including epoxide (=O) and hydroxyl (-OH) on its flat surface, and carbonyl (-C=O) and carboxyl (-COOH) on its edges, which enable it to form connections with a variety of organic and inorganic materials **[1].** This happens through non-covalent, covalent, and ionic interactions, creating new hybrids and composites with special properties. The possibility of bandgap modification in GO is of interest for its execution in photonic and electronic devices **[2]**. Researchers found that GO nanosheets, prepared by pulsed laser ablation in

liquid (PLAL), are photoluminescent and biocompatible, making them suitable for bioimaging applications. Fe_3O_4 is gaining a lot of attention because of its unique structural characteristics. The distribution of cations between its sites and their exchange interaction provides superior optical, electrical, electronic, and magnetic properties [3]. Fe_3O_4 is the most magnetic of all the naturally occurring metals on Earth; it has garnered a lot of interest; also, it is non-toxic and biocompatible. Moreover, noble metal nanoparticles, like gold (Au), have drawn a lot of interest due to their unique physical characteristics, especially their pronounced plasmon absorption peaks in the visible spectrum. The size, shape, and stability of the particles over time all affect the resonance frequencies. The demonstrated absorbance demonstrates a promising strategy to boost the efficacy of diverse cancer treatments. Researchers have invested significant effort in developing a multifunctional nanomaterial, aiming to achieve multiple properties in a single material [4]. These materials consist of at least two unique materials, each possessing specific properties from their respective segments [5]. There are several chemical methods available for obtaining nanomaterials. However, the purity of the finished nanomaterials—that is, their absence of impurities and precursor residues—is crucial for many applications [2]. Researchers have recently been actively exploring high-energy physical methods for nanoparticle production. Among these techniques is pulsed laser ablation in a liquid (PLAL). This method enables the direct production of particles in the form of colloids in pure liquids with either no precursors or very few [9]. Furthermore, it is an approach for micro-/nanostructure generation directly from bulk materials [7]. When the laser beam focuses on the surface of a solid target material in the surrounding media (gas or liquid), it rapidly raises the temperature of the irradiated spot, vaporizing the target material. When evaporating species (atoms and clusters) collide with nearby molecules, they create a laser-induced plasma plume by exciting the electron state, emitting light, and generating electrons and ions [3]. The target material, surrounding media, ambient pressure, and laser settings all influence the plasma structures, including the size of the plume and its emission spectrum. The process of laser ablation in liquid confines the plasma plume in a small region, thereby directly producing nanoparticles in the liquid phase [8]. In this work, the NGOs were prepared by Nd:YAG pulsed laser in 20 ml of deionized water for 60 min. Au/Fe_3O_4NCs were also prepared the same way and then loaded on NGOs to obtain Au/Fe_3O_4/GO NCs. The prepared samples were characterized by transmission electron microscopy (TEM), Fourier transform infrared spectroscopy (FTIR), and UV-visible absorption spectroscopy. The absorption curve we got was used to analyze the optical features of the samples. This includes the bandgap (E_g), optical conductivity (σ), absorption coefficient (α), Urbach energy (E_U), electronegativity (Δx), refractive index (n), steepness parameter (σ_s), electron-phonon interaction ($E_{e\text{-}p}$), electronic polarizability (αe), molar volume (V_m), molar refraction (R_m), and molar electronic polarizability (α_{me}).

1. Experimental

a. Synthesis of GO, Fe_3O_4/GO, and Au/Fe_3O_4/GO NCs

We first put the graphite rod from Sigma Aldrich in an ultrasonic bath for 10 min and then we used deionized water to wash it. The rod was fixed at the bottom of 20 ml of distilled water, and then the Q-switched Nd:YAG laser with a wavelength of 1064 nm, pulse width (8-12) ns, repetition rate of 10 Hz and 450 mj was focused on the graphite target by a converging lens of 10 cm focal length for 60 min; a solution of GO nanosheets was simply formed.

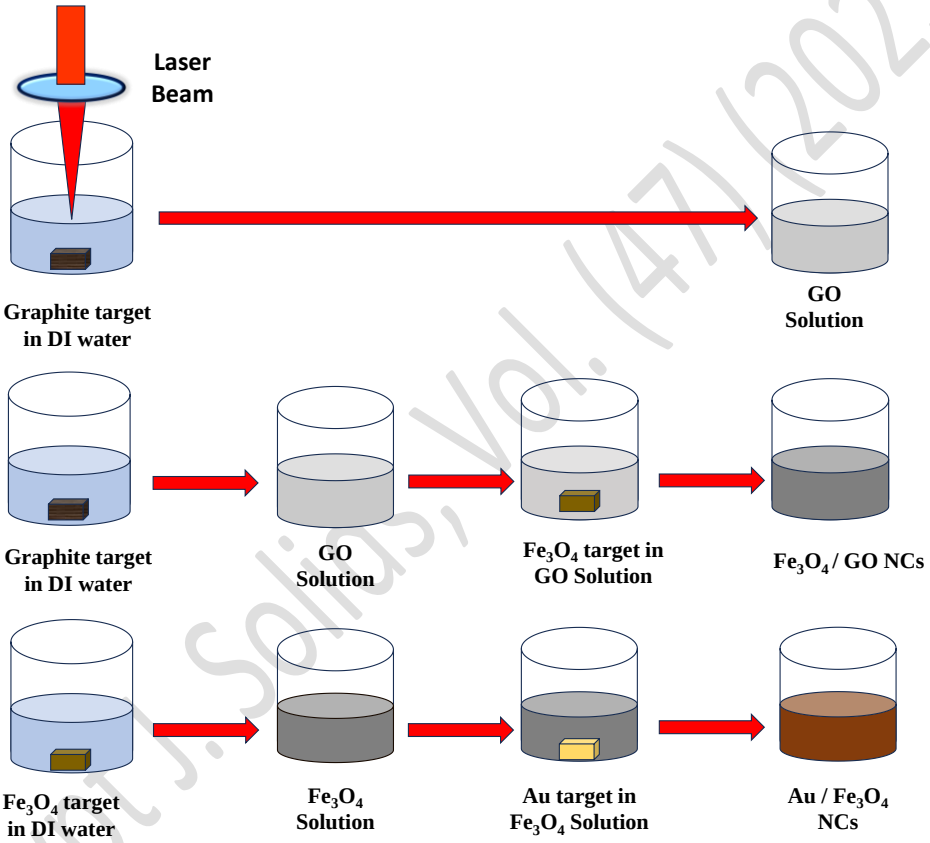

Fig.1. Shows the schematic diagram of the laser ablation technique.

Fe_3O_4 cube was supplied from (SAMMLUNG VON), and a high-purity Au slab (99.99%) from Sigma Aldrich was also cleaned in the same way as graphite. Fe_3O_4/GO has been obtained by immersing Fe_3O_4 cubes in GO solution and ablating them by laser for 30 min. Also, Au/Fe_3O_4 NCs were prepared by the same technique; first, Fe_3O_4 cubes were immersed at 20 ml below the distilled water surface and radiated for 5 min, then Au slabs were fixed at the bottom of the Fe_3O_4 solution and ablated for 45 min, resulting in the production of Au/Fe_3O_4 NCs. The Au/Fe_3O_4 and GO solutions were mixed by volume ratio 1:3 and sonicated for 30 min to accelerate the reaction to form Au/Fe_3O_4/GO.

Finally, the three samples were obtained: GO NPs, Fe_3O_4/GO NCs, and Au/Fe_3O_4/GO NCs. The experimental setup is shown in **Fig. 1**. All samples were prepared at ambient temperature and pressure.

b. Characterization tools

Nd:YAG laser from The Quanta-Ray® Lab series, the used model is (Quanta Ray) Lab-150.The size and morphology of NPs were identified using a high-resolution transmission electron microscope (HRTEM) (JEOL-JEM-2100 Plus, Japan). Scan images were recorded at an acceleration voltage of 200 kV. The functional groups present in the samples were identified using Fourier transform infrared (FT-IR) (Bruker ALPHA II, Germany), and the optical absorption spectrum of the samples was measured in the 200–600 nm wavelength range using quartz cells with a 1 cm optical path length using a JASCO 670 UV-vis spectrophotometer (Japan). Sonicator type EQ-VGT-1613QTD from MTI.

3. Results and discussion.

a) Transmission electron microscopy

TEM images of prepared GO nanosheets, Fe_3O_4/GO NCs, and Au/Fe_3O_4/GO NCs are shown in **Fig. 2** (a, b, and c), respectively.

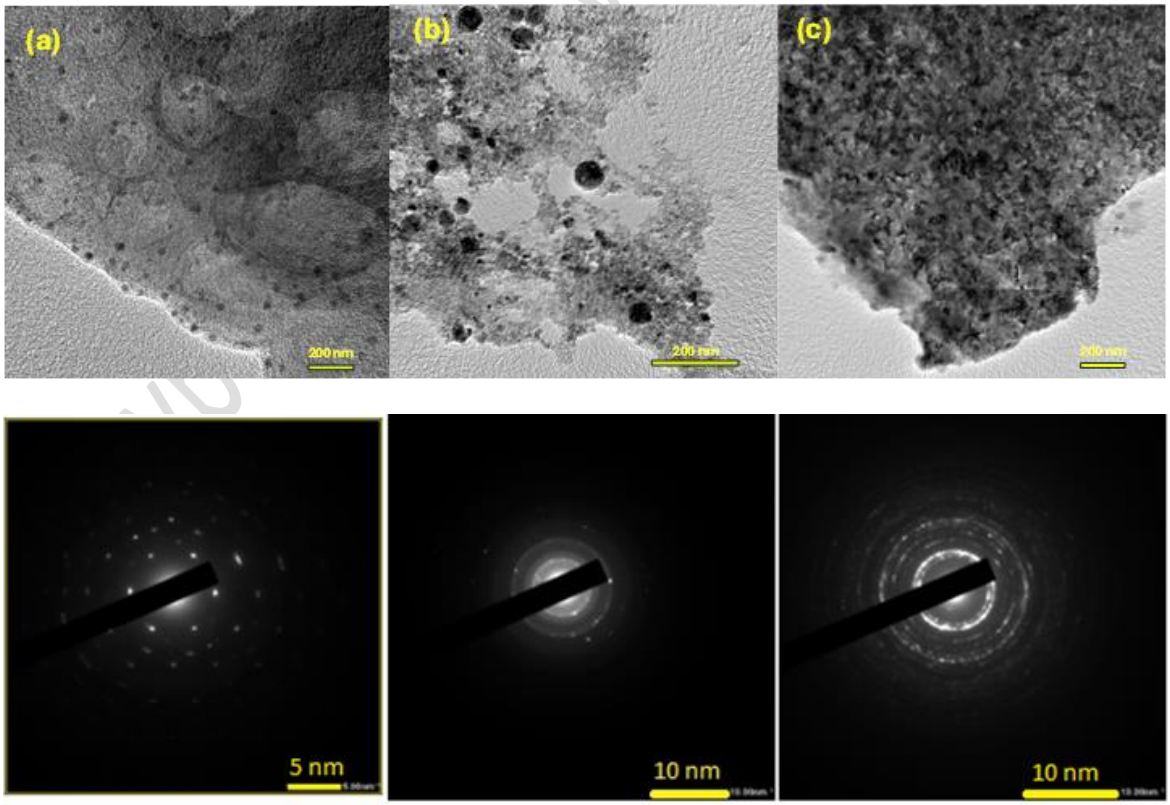

***Fig.2** Shows the TEM images of GO, Fe_3O_4/GO and Au/ Fe_3O_4/GO NCs and SAED Patterns.*

They reveal the crumpled nature; it's possible that some agglomeration happened when the samples were drying on the TEM grid. It is observed that GO was formed as an irregular thin layer. The non-deformed nanosheets help the charge carriers to transform fast with less energy, leading to a high interaction with the surrounding **[4]**. It is easily observed that some dots were found at **Fig. 2(a)** that were not observed at lower resolution, our result matching with **[6]**. In their work, laser ablation of a graphite target led to obtaining porous graphene sheets as primary products and graphene quantum dots (GQDs) as secondary products. We estimate the lattice spacing to be 0.29 nm. Our result is in good agreement with **[7]**, where laser-ablated GQDs have a lattice spacing larger than chemically oxidized GQDs, which is nearly in the range of 0.3 nm. They attribute the grater lattice spacing of the laser-ablated GQDs **[29].** The increased hydroxyl group relative concentration causes the carbon backbone gap to widen. **Fig. 2(a1)** shows the SAED pattern of GO which reveals the mono crystal structure. Fe_3O_4/GO NCs with different resolution are shown in the **Fig.2(b)**. Fe_3O_4 nanoparticles in a spherical shape have been loaded on the GO surface. A wide range of particle size distributions with average particle sizes nearly 51.64 nm are shown in **Fig 2(b)**. **Fig 2(c)** illustrates that Au/Fe_3O_4/GO NCs, where Au/Fe_3O_4 NCs diffused completely in GO sheets, and its shape is no longer recognized, which reveals the effect of sonication that accelerates the combination. This acceleration is due to either physical or chemical effects of cavitation **[8]**. Where **Fig 2(b1, c1)** show the SAED patterns for Fe_3O_4/GO and Au/Fe_3O_4/GO NCs multi crystal structure nature.

b) Fourier transform infrared spectroscopy (FTIR)

The FT-IR spectrum of GO, Fe_3O_4/GO, and Au/Fe_3O_4/GO is shown in the **Fig.3.** The three curves clearly display similar absorption bands. The broad band that starts from (3683) up to (2980) cm^{-1} could be assigned to the absorbed water molecules over the nanoparticles **[9]**. GO Spectrum confirmed the presence of carboxyl COOH (1422 cm^{-1}); the band at 1636 cm^{-1} is assigned to the bending mode of the unsaturated carbon double bond (C=C), and the one at 1038 cm^{-1} belongs to the stretching vibration of alkoxy C-O functional groups. For the Fe_3O_4/GO composite, it differs from that of GO by the disappearance of some oxygen groups, indicating some reduction that took place in graphene oxide sheets **[10]**. Moreover, the peak at (582 cm^{-1}) assigned to the Fe-O stretching modes of the magnetite lattice and two peaks at (425 cm^{-1}) and (682 cm^{-1}) suggest a cation vacancy arrangement that is creating a reduced symmetrical structure, most likely because of surface oxidation **[11]**. These peaks suggest that the Fe3O4 NSs were effectively decorated on the surface of GO. For Au/Fe_3O_4/GO, besides the GO bands and Fe-O bands, two peaks at (2938 cm^{-1}) and (2852 cm^{-1}) indicate C-H stretching alkane and C-H stretching aldehyde, respectively **[22]**. The weak bands at (1248 cm^{-1}) and (1038 cm^{-1}) show C-N stretching of aliphatic amines and C-O stretching of carboxylic amines, respectively **[12]**. It confirmed the successful attachment of Au nanoparticles to the Fe_3O_4/GO NCs.

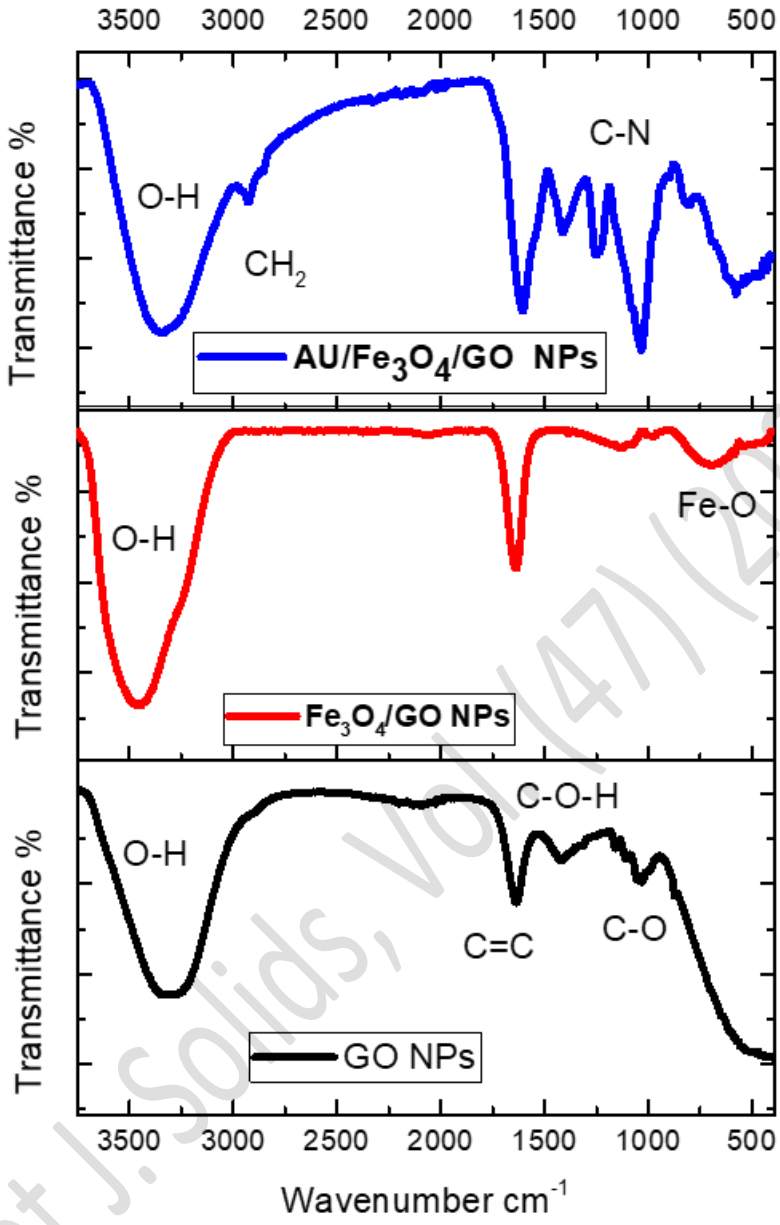

Fig.3. The FT-IR spectra of GO, Fe3O4/GO and AU/ Fe3O4/GO NCs.

c) Optical properties studies

Fig 4-a represents the optical absorption intensity of GO, Fe_3O_4/GO and Au/ Fe_3O_4/GO NCs as a function of the wavelength.

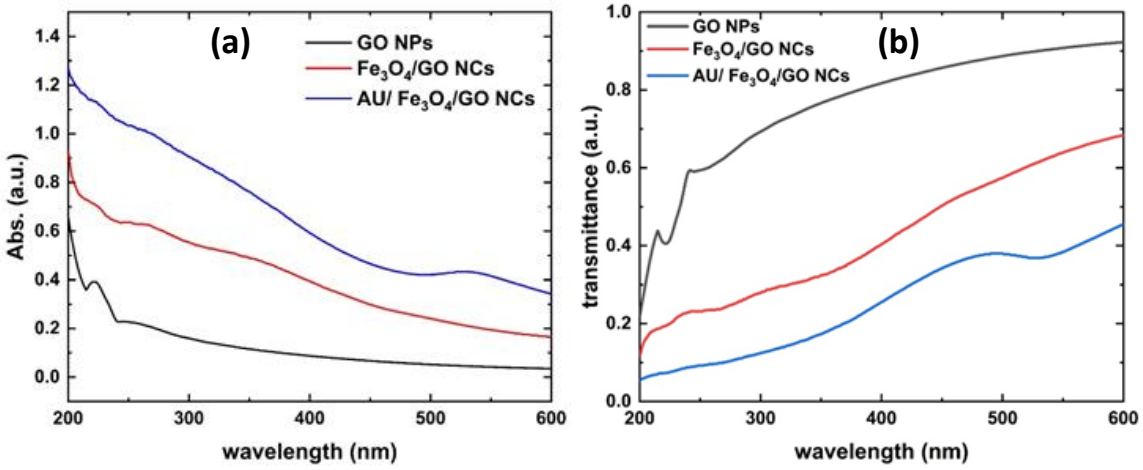

Fig.4, ***a) Absorption spectra of GO, Fe_3O_4/GO and Au/ Fe_3O_4/GO NCs b) Transmission spectra of GO, Fe_3O_4/GO and Au/ Fe_3O_4/GO NCs.***

It is observed that in the case of GO spectra, the characteristics peak at 222 nm due to the aromatic transition of π-π* belonging to the C-C bond, and another peak at nearly 265 nm corresponds to the n-π* transition [7]. Adding Fe_3O_4 to GO and irradiating it with a laser again, the GO peak started to make a red shift of the absorption peak relative to the π-π* transitions, meaning a repairing of the sp^2 hybridization, which means some reduction of oxygen groups [13], as well as the interaction between Fe_3O_4 and GO. The absorption spectrum of Au/Fe_3O_4/GO NCs shows an increase in the absorption intensity; this is because under light excitation, localized surface plasmon resonance (LSPR) of gold dominates. The observed peak at 530 nm corresponds to surface plasmon of Au-decorated Fe_3O_4 [14]. **Fig 4(b)** shows the transmission curve of GO, Fe_3O_4/GO, and Au/Fe_3O_4 NCs; the figure reveals that the transmission decreases by adding Fe_3O_4 NPs and Au/Fe_3O_4 NCs. The absorption coefficient (α) of GO, Fe_3O_4/GO, and Au/Fe_3O_4/GO NCs as a function of incident light energy were calculated and given in **Fig. 5(a) [15]**.

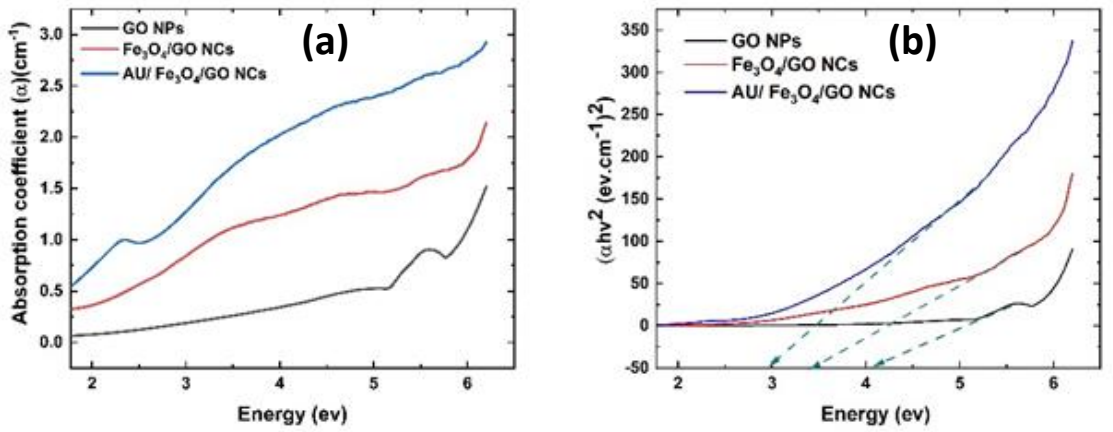

Fig.5, a) Absorption coefficient curve of GO, Fe_3O_4/GO and AU/ Fe_3O_4/GO NCs. b) Variation of $(\alpha hv)^2$ with the photon energy (hv)of GO, Fe_3O_4/GO and AU/ Fe_3O_4/GO NCs.

It shows that the decorated GO nanosheets have a much higher optical absorption coefficient than pure GO nanosheets, which indicates the high absorption nature of the nano Fe_3O_4 and Au/Fe_3O. α and photon energy (hν) are related to each other by Tauc's equation as [2]:

$$(\boldsymbol{\alpha h\nu})^{\frac{1}{n}} = \boldsymbol{\beta}\left(\boldsymbol{h\nu - E_g}\right) \qquad (1)$$

Since β is a band tailing parameter, E_g is optical band gap energy, and n is the power factor of the transition mode. The range of n (0.3-0.8) indicates the electronic permitted direct transition [17]. The bandgap values are established by analyzing the Tauc-plot curve of the $(\alpha h\nu)^2$ value on (hν). By intercepting this linear part's extrapolation to the energy axis, we obtain the energy bandgap E_g [18]. Plotting $(\alpha h\nu)^2$ against photon energy (hν) for all the samples is displayed in Figure 5-b. The values of E_g for GO, Fe_3O_4/GO, and Au/Fe_3O_4/GO NCs are 4.1 eV, 3.4 eV, and 3 eV, respectively. The presence of different oxidation states of iron in the magnetite (Fe^{2+} and Fe^{3+}) could also introduce specific impurity states, particularly in the electronic structure of the material, altering the conductivity or introducing new energy levels within the band gap. Also, interaction between the graphene oxide, magnetite and gold could lead to charge transfer between the three materials, creating localized states in the graphene's conduction or valence bands. The iron atoms in magnetite can also interact with the carbon atoms in graphene, leading to hybridized electronic states at the interface, which could behave as impurity states._ Because of this, the doped material's bandgap energy narrows, and it absorbs photons with bandgap energies between 3 and 4.1 eV, which causes more excited electrons to remain inside the doped sheets' conduction band. Urbach energy is calculated by the following equation: [16][19].

$$\boldsymbol{ln\alpha = ln\alpha_o + \frac{h\nu}{E_U}} \qquad (2)$$

αo is a constant and E_U is the band tail width (Urbach energy) of the localized states in the optical energy gap. We have determined the Eu by calculating the equation's inverse slope **(2)**. **Table 1** tabulates the value of the band tailing. The relation between E_g and band E_U is shown in **Fig 6 (a)** for the three samples. It is clearly observed that by the addition of nanoparticles to GO sheets, the weak bonds of oxygen are replaced by decorating material. Increasing in the $\mathbf{E_U}$ value ashore that a broadening in localized states in the forbidden gap led to a decrement in it [22].

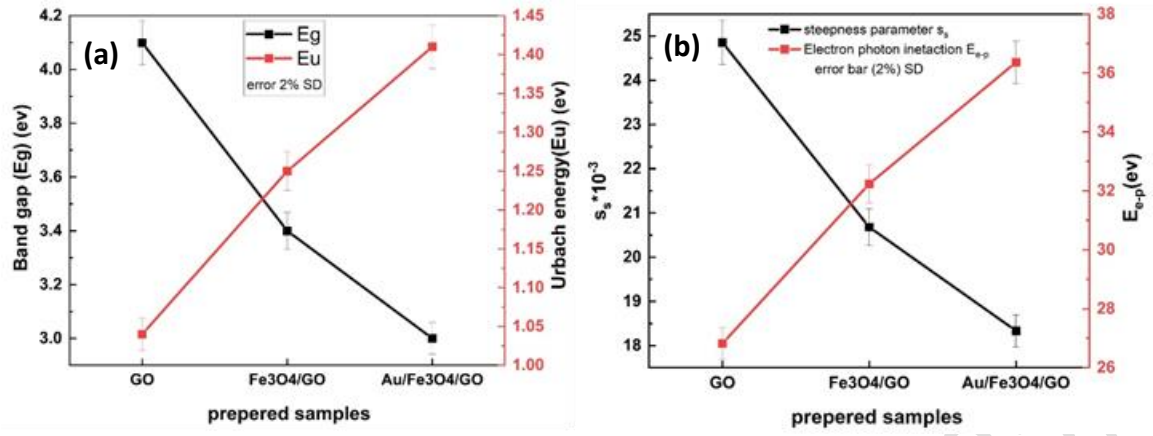

Fig.6. a) Variation of the optical band gap (E g) and Urbach energy (E u) of GO, Fe3O4/GO and Au/ Fe3O4/GO NCs. b) Variation of both steepness parameter (σs) and electron-phonon interaction (Ee−p) of GO, Fe3O4/GO and Au/ Fe3O4/GO NCs.

The steepness parameter (σ_s), which demonstrates the widening of the absorption band, can be calculated empirically using this equation: [20] [22].

$$\sigma_s = {K_B T}/{E_U} \qquad (3)$$

We define k_B as the Boltzmann constant and T as the absolute temperature. Furthermore, σ_s determines how strongly the electron-phonon interacts (Ee-p), and they related to one another by the relationship: [21]

$$\mathbf{E_{e-p} = \frac{2}{3\sigma s}} \qquad (4)$$

The σ_s and E_{e-p} values were calculated using equations (3) and (4), respectively, and tabulated in **Table 1**. The plot of the three prepared samples versus the three prepared samples is shown in **Fig. 6.** The s decreases as the E_{e-p} increases. The total electronegativity difference ($\Delta\chi$) is an important parameter to understand the chemical bonding. You can obtain the value of (E_g) by substituting it into the Duffy relation: [21]

$$\Delta X = \mathbf{0.2688} E_g \qquad (5)$$

Where ($\Delta\chi$) value decreased from 1.04 to 0.806 as calculated in table 1. Finding the refractive indices of materials is crucial, particularly for those that can be utilized to make any kind of optical device, such as switches, filters, modulation, etc. Many relations are presented between the refractive index (n), (E_g) and ($\Delta\chi$) shown in the following relations [22][23]: The value decreased from 1.04 to 0.806 in **Table 1**.

Table 1 contains the calculated values for the refractive index (n). The average refractive index (n_{avg}) was increased, assures the inverse proportional relation between E_g and n.

Also, materials with small n are transparent in the visible region where the sample's colour becomes gradually darker.

$$n = -\ln(0.027E_g) \quad (6)$$

$$n = \sqrt{\left(\sqrt[6]{\frac{5}{E_g}} - 2\right)} \quad (7)$$

$$n = -\ln(0.102\Delta X) \quad (8)$$

***Table 1**: Bandgap (E_g), Urbach energy (Eu), electronegativity (ΔX), refractive index (n), steepness parameter (σs), electron phonon interaction (Ee-p) of GO, Fe3O4/GO and Au/ Fe3O4/GO NC respectively.*

Samples	E_g (ev)	Eu (ev)	ΔX	Equation (n)			Average(n) (n_{avg})	σ_s	E_{e-p}
				Eq (6)	Eq (7)	Eq (8)			
GO	4.1	1.04	1.102	2.2	2.15	2.18	2.17	24.8	26.8
Fe_3O_4/GO	3.4	1.25	0.913	2.38	2.29	2.37	2.39	20.6	32.2
Au/ Fe_3O_4/GO	3	1.41	0.806	2.51	2.39	2.49	2.46	18.33	36.36

The optical response is studied for the samples in terms of optical conductivity calculated using the following relation:[3]

$$\sigma = \frac{\alpha n c}{4\pi} \quad (9)$$

Since (**c**) is the speed of light in vacuum, **Fig.7** gives optical conductivity as a function of the photon energy. The optical conductivity is higher at larger photon energy due to higher electron excitation at this energy, and the conductivity of decorated GO sheets is higher than pure GO sheets, which reveals the high photo-response **[24]**. Using the values of n_{avg} obtained in **Table 1**, the electronic polarizability can be calculated by using in the following equation: **[22] [25]**

$$\alpha_e = \frac{3(n_{avg}^2 - 1)}{4\pi N_A(n_{avg}^2 + 2)} \quad (10)$$

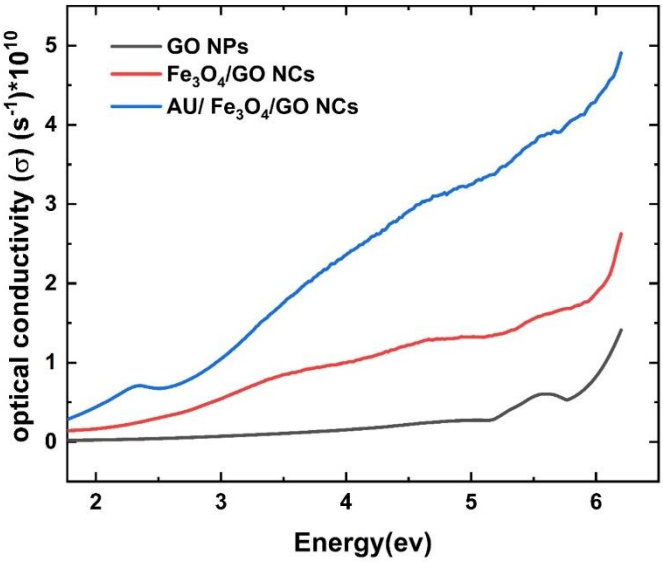

Fig.7, optical conductivity spectrum of GO, Fe_3O_4/GO and AU/ Fe_3O_4/GO NC.

$\mathbf{V_m}$ is the molar volume, can be evaluated by the electronic polarizability ($\boldsymbol{\alpha_e}$) and by substitution in the following relation: [4]

$$\alpha_e = 0.395\left(\frac{n_{avg}^2 - 1}{n_{avg}^2 + 1}\right)V_m \qquad (11)$$

$\mathbf{R_m}$ is the molar refraction, which calculated based on the value of the average refractive index and molar volume by the Volf and Lorentz-Lorenz formula: [5][6]

$$R_m = \left(\frac{n_{avg}^2 - 1}{n_{avg}^2 + 1}\right)V_m \qquad (12)$$

$\boldsymbol{\alpha_{me}}$ is the molar electronic polarizability, which given by: [5]

$$\alpha_{me} = \frac{R_m}{2.52} \qquad (13)$$

The obtained values of (α_e), (V_m), (R_m) and (α_{me}) are present in **Table 2**.

Table 2: Electronic polarizability (α_e), molar volume (v_m), molar refraction (R_m) and molar electronic polarizability (α_{me}) of GO, Fe_3O_4/GO and Au/ Fe_3O_4/GO NC respectively.

Samples	α_e*10^{-25}	V_m *10^{-25}	R_m*10^{-25}	α_{em}*10^{-25}
GO	2.20	8.55	4.75	1.88
Fe_3O_4/GO	2.38	8.71	4.83	1.92
Au/ Fe_3O_4/GO	2.49	8.80	4.89	1.94

It's clearly seen that by the addition of Fe_3O_4 NPs and Au/Fe_3O_4 NCs, the electronic polarizability increased. There is a general thought by which the electronic polarizability of samples containing oxide ion increases with increasing refractive index and decreasing energy gap [27]. The (V_m), (R_m), and (α_{me}) are proportionally related to (α_e), so they also increased.

4.Conclusion

GO, Fe_3O_4/GO, and Au/Fe_3O_4/GO NCs were successfully prepared by a powerful green PLAL technique. The TEM image showed that the samples had uneven, flat layers of GO, which were evenly covered with Fe_3O_4 particles that are about 51.64 nm in size. Finally, by adding Au/Fe_3O_4 NCs to the GO solution, they diffused completely with the aid of sonication. The FT-IR spectrum confirms the functional groups of GO, Fe_3O_4, and Au/Fe_3O_4, as well as the bonds that have been built between them. The UV-visible spectrum indicates a red shift in the absorption edge of each of the three samples. The (E_g) decreased from 4.1 to 3 eV and (α, E_U, n, σ, α_e, V_m, R_m, α_{em}, and E_{e-p}) all increased for the three samples, respectively due to introducing new impurity energy levels, where (σ_s and Δx) decreased. This shows that our structure is applicable for different applications, such as photonic applications, drug delivery applications, and water treatment applications [28].

References

[1] J. M. Jassim, M. S. Al-samak, W. T. Younes, and H. Kisov, "Near-Infrared Plasmonic Random Laser Emission Employing Gold Nanorods and LDS-821 Dye," Plasmonics, 2025, **doi: 10.1007/s11468-025-02765-3**.

[2] A. Okasha, M. B. Mohamed, S. Negm, and H. Talaat, "Weak exciton-plasmon and exciton-phonon coupling in chemically synthesized Ag/CdSe metal/semiconductor hybrid nanocomposite," *Phys. E Low-Dimensional Syst. Nanostructures*, vol. 44, no. 10, pp. 2094–2098, 2012, **doi: 10.1016/j.physe.2012.06.022**.

[3] K. Easawi, M. Nabil, T. Abdallah, S. Negm, and H. Talaat, "Plasmonic Absorption Enhancement in Au/CdS Nanocomposite," *World Acad. Sci. Eng. Technol.*, vol. 6, no. 1, pp. **63–66, 2012**.

[4] A. Hellal, H. Abdelsalam, W. Tawfik, and M. A. Ibrahim, "Assessment of doped graphene in the removal of atrazine from water," Sci. Rep., vol. 14, no. 1, pp. 1–17, 2024, **doi: 10.1038/s41598-024-71886-2**.

[5] P. Hajipour, A. Bahrami, A. Eslami, A. Hosseini-Abari, and H. reza Hagh Ranjbar, "Chemical bath synthesis of CuO-GO-Ag nanocomposites with enhanced antibacterial properties," *J. Alloys Compd.*, vol. 821, p. 153456, 2020, **doi: 10.1016/j.jallcom.2019.153456.**

[6] P. Russo, R. Liang, E. Jabari, E. Marzbanrad, E. Toyserkani, and Y. Zhou, "Single-step synthesis of graphene quantum dots by femtosecond laser ablation of graphene oxide dispersions," Nanoscale, vol. 8, no. 16, pp. 1–15, Mar. 2016, **doi: 10.1039/C6NR01148A**.

[7] R. L. Calabro, D. S. Yang, and D. Y. Kim, "Liquid-phase laser ablation synthesis of graphene quantum dots from carbon nano-onions: Comparison with chemical oxidation," *J. Colloid Interface Sci.*, vol. 527, pp. 132–140, 2018, **doi: 10.1016/j.jcis.2018.04.113.**

[8] A. Pradhan, R. C. Jones, D. Caruntu, C. J. O'Connor, and M. A. Tarr, "Gold–magnetite nanocomposite materials formed via sonochemical methods," Ultrason Sonochem, vol. 15, no. 5, pp. 891–897, 2008, **doi: https://doi.org/10.1016/j.ultsonch.2008.01.004.**

[9] N. M. Dat et al., "Synthesis of silver/reduced graphene oxide for antibacterial activity and catalytic reduction of organic dyes," Synth Met, vol. 260, no. 116260, pp. 1–10, 2020, **doi: https://doi.org/10.1016/j.synthmet.2019.116260**.

[10] Y. Yuan, W. Jiang, Y. Wang, P. Shen, F. Li, and P. Li, "Applied Surface Science Hydrothermal preparation of Fe 2 O 3 / graphene nanocomposite and its enhanced catalytic activity on the thermal decomposition of ammonium perchlorate," *Appl. Surf. Sci.*, vol. 303, pp. 354–359, 2014, **doi: 10.1016/j.apsusc.2014.03.005**.

[11] A. G. Roca, J. F. Marco, M. del P. Morales, and C. J. Serna, "Effect of Nature and Particle Size on Properties of Uniform Magnetite and Maghemite Nanoparticles," The Journal of Physical Chemistry C, vol. 111, no. 50, pp. 18577–18584, Dec. 2007, **doi: 10.1021/jp075133m.**

[12] S. Rajeshkumar, "Anticancer activity of eco-friendly gold nanoparticles against lung and liver cancer cells," *J. Genet. Eng. Biotechnol.*, vol. 14, no. 1, pp. 195–202, 2016, **doi: 10.1016/j.jgeb.2016.05.007**.

[13] P. Russo, L. D'Urso, A. Hu, N. Zhou, and G. Compagnini, "In liquid laser treated graphene oxide for dye removal," Appl Surf Sci, vol. 348, pp. 85–91, 2015, doi: https://**doi.org/10.1016/j.apsusc.2014.12.014**.

[14] A. S. Wasfi, H. R. Humud, and N. K. Fadhil, "Synthesis of core-shell Fe3O4-Au nanoparticles by electrical exploding wire technique combined with laser pulse shooting," *Opt. Laser Technol.*, vol. 111, pp. 720–726, 2019, **doi: 10.1016/j.optlastec.2018.09.006**.

[15] S. S. Fouad, E. Baradács, M. Nabil, B. Parditka, S. Negm, and Z. Erdélyi, "Microstructural and optical duality of TiO2/Cu/TiO2 trilayer films grown by atomic

layer deposition and DC magnetron sputtering," Inorg Chem Commun, vol. 145, pp. 1-7, 2022, doi: https://**doi.org/10.1016/j.inoche.2022.110017**.

[16] A. S. Hassanien and A. A. Akl, "Influence of composition on optical and dispersion parameters of thermally evaporated non-crystalline Cd50S50-xSex thin films," *J. Alloys Compd.*, vol. 648, pp. 280–290, Jul. 2015, **doi: 10.1016/j.jallcom.2015.06.231**.

[17] N. M. El-Shafai *et al.*, "Magnetite nano-spherical quantum dots decorated graphene oxide nano sheet (GO@Fe3O4): Electrochemical properties and applications for removal heavy metals, pesticide and solar cell," *Appl. Surf. Sci.*, vol. 506, Mar. 2020, **doi: 10.1016/j.apsusc.2019.144896.**

[18] F. Horia, K. Easawi, R. Khalil, S. Abdallah, M. El-Mansy, and S. Negm, "Optical and Thermophysical Characterization of Fe3O4nanoparticle," in *IOP Conference Series: Materials Science and Engineering*, IOP Publishing Ltd, Oct. 2020. **doi: 10.1088/1757-899X/956/1/012016.**

[19] M. H. MAMAT, M. Z. SAHDAN, S. AMIZAM, H. A. RAFAIE, Z. KHUSAIMI, and M. RUSOP, "Optical and electrical properties of aluminum doped zinc oxide thin films at various doping concentrations," Journal of the Ceramic Society of Japan, vol. 117, no. 1371, pp. 1263–1267, 2009, **doi: 10.2109/jcersj2.117.1263**.

[20] Z. El-Qahtani, A. Badawi, K. Easawi, N. Al-Hosiny, and S. Abdallah, "Photoacoustic study of optical and thermal properties of alloyed CdTe xS1-x nanocrystals," *Mater. Sci. Semicond. Process.*, vol. 20, no. 1, pp. 68–73, 2014, **doi: 10.1016/j.mssp.2013.12.034.**

[21] M. Nabil, H. F, S. S. Fouad, and S. Negm, "Impact of Au nanoparticles on the thermophysicalparameters of Fe3O4 nanoparticles for seawater desalination," *Opt. Mater. (Amst).*, vol. 128, no. April, p. 112456, 2022, **doi: 10.1016/j.optmat.2022.112456**.

[22] M. Nabil, S. S. Fouad, K. Easawi, S. Abdallah, and H. F, "Novel correlations between optical absorption and water desalination of Ag/Fe3O4 nanocomposite prepared by pulsed laser ablation in liquid," *Opt. Laser Technol.*, vol. 164, no. April, 2023, **doi: 10.1016/j.optlastec.2023.109545.**

[23] M. Nabil, F. Horia, S. S. Fouad, and S. Negm, "Impact of Au nanoparticles on the thermophysicalparameters of Fe 3 O 4 nanoparticles for seawater desalination," *Opt. Mater. (Amst).*, vol. 128, no. May, p. 112456, 2022, **doi: 10.1016/j.optmat.2022.112456.**

[24] S. S. Fouad, I. M. El Radaf, P. Sharma, and M. S. El-bana, "Multifunctional CZTS thin fi lms : Structural , optoelectrical , electrical and photovoltaic properties," *J. Alloys Compd.*, vol. 757, pp. 124–133, 2018, **doi: 10.1016/j.jallcom.2018.05.033**.

[25] S. A. Umar, M. K. Halimah, K. T. Chan, and A. A. Latif, "Polarizability, optical basicity and electric susceptibility of Er3 + doped silicate borotellurite glasses," *J. Non. Cryst. Solids*, vol. 471, no. March, pp. 101–109, 2017, **doi: 10.1016/j.jnoncrysol.2017.05.018.**

[26] V. Dimitrov and T. Komatsu, "An Interpretation Of Optical Properties Of Oxides And Oxide Glasses In Terms Of The Electronic Ion Polarizability And Average Single Bond Strength (Review)," Journal of the University of Chemical Technology and Metallurgy, vol. 45, no. 3, pp. 219–250, 2010, [Online]. Available: **https://api.semanticscholar.org/CorpusID:53958785**.

[27] V. Dimitrov and T. Komatsu, "Electronic polarizability, optical basicity and non-linear optical properties of oxide glasses," *J. Non. Cryst. Solids*, vol. 249, no. 2–3, pp. 160–179, 1999, **doi: 10.1016/S0022-3093(99)00317-8**.

[28] A. A. Menazea et al., "Chitosan/graphene oxide composite as an effective removal of Ni, Cu, As, Cd and Pb from wastewater," Comput. Theor. Chem., vol. 1189, no. April, 2020, **doi: 10.1016/j.comptc.2020.112980**.

[29] A. Hellal, H. Abdelsalam, W. Tawfik, and M. A. Ibrahim, "Removal of Atrazine from contaminated water by functionalized graphene quantum dots," Opt. Quantum Electron., vol. 56, no. 3, pp. 1–16, 2024, **doi: 10.1007/s11082-023-05909-z**.